

## Article

# Preparation and Properties of Expansive Backfill Material Based on Municipal Solid Waste Incineration Fly Ash and Coal Gangue

Zhen Wang<sup>1,\*</sup>, Honglin Liu<sup>2</sup>, Yuanxin Zhang<sup>3</sup>, Zhiwen Chen<sup>1,\*</sup>, Rumeng Zhao<sup>4</sup>, Yongyong Jia<sup>1</sup>, Mingchao Yong<sup>1</sup> and Guodong Li<sup>2</sup>

<sup>1</sup> Institute of Coal Science, Xinjiang Uygur Autonomous Region, Urumqi 830091, China; jiayy@163.com (Y.J.); mingchaoyong1992@163.com (M.Y.)

<sup>2</sup> College of Geology and Mines Engineering, Xinjiang University, Urumqi 830046, China; liuhonglin@xju.edu.cn (H.L.); cklgd2011@xju.edu.cn (G.L.)

<sup>3</sup> School of Finance and Financial Management, Zhengzhou Technical College, Zhengzhou 450121, China; zhangyuanxinmi@163.com

<sup>4</sup> School of Environmental Engineering, Henan University of Technology, Zhengzhou 450001, China; meng210223515@163.com

\* Correspondence: mks\_403@163.com (Z.W.); chen\_zhiwen@stu.xju.edu.cn (Z.C.); Tel.: +86-1519-902-6971 (Z.W.); +86-1788-116-7054 (Z.C.)

**Abstract:** To realize the large-scale utilization of municipal solid waste incineration (MSWI) fly ash in the field of building materials and to reduce the cost of coal mine backfill mining, the effects of the mixing ratio of cementitious materials, the particle size distribution of aggregates, and the amount and mass concentration of cementitious materials on the properties of backfill materials were experimentally investigated, and the microstructure of the hydration products was analyzed. The results showed that as the mass ratio of MSWI fly ash to bottom ash increased, the rate of expansion of the cementitious system continued to increase, and the compressive strength of the cementitious system continued to decrease. The Al (aluminum) and AlN (aluminum nitride) in the fly ash reacted with water to generate gas, causing the expansion of the cementitious materials; NaOH increased the alkalinity of the solution, which promoted the formation of more bubbles, thereby improving the expansion performance of the cementitious material. When the content of NaOH was 0.9%, the sample rate of expansion could reach 15.9%. The addition of CaCl<sub>2</sub> promoted the early hydration reaction of the cementitious material, forming a dense microstructure, thus improving the early strength and rate of expansion of the cementitious material. The compressive strength of the backfill body increased as the fractal dimension of the aggregate particles increased, and the particle grading scheme of group S1 was optimal. The 1-day, 3-day, and 28-day strengths of the backfill body of group S1 reached 0.72 MPa, 1.43 MPa, and 3.26 MPa, respectively. It is recommended to choose a backfill paste concentration ranging between 78.5% and 80% and a reasonable amount of cementitious material between 20% and 25%. After the MSWI fly ash was prepared as a backfill material, the leaching of potentially harmful elements in the fly ash was greatly reduced, and the concentration of dioxin was reduced to 13 ng TEQ/kg. This was attributed to the dilution of the cement, the physical encapsulation of gel products, and the isomorphous replacement of Ca<sup>2+</sup> in calcium aluminate chloride hydrate.

**Keywords:** municipal solid waste incineration fly ash; coal gangue; backfill material; micro-analysis; heavy metal leaching



**Citation:** Wang, Z.; Liu, H.; Zhang, Y.; Chen, Z.; Zhao, R.; Jia, Y.; Yong, M.; Li, G. Preparation and Properties of Expansive Backfill Material Based on Municipal Solid Waste Incineration Fly Ash and Coal Gangue. *Minerals* **2024**, *14*, 513. <https://doi.org/10.3390/min14050513>

Academic Editor: Abbas Taheri

Received: 11 March 2024

Revised: 10 May 2024

Accepted: 12 May 2024

Published: 14 May 2024



**Copyright:** © 2024 by the authors. Licensee MDPI, Basel, Switzerland. This article is an open access article distributed under the terms and conditions of the Creative Commons Attribution (CC BY) license (<https://creativecommons.org/licenses/by/4.0/>).

## 1. Introduction

In 2022, the amount of municipal solid waste in China exceeded 250 million tons, showing an increasing trend year by year. The recommended treatment methods for domestic waste are sanitary landfill, incineration, and composting. The incineration method shows the significant advantages of reducing the amount of waste and being harmless, and

it is the recommended treatment method adopted by most countries in the world [1–4]. However, 10% to 15% of the waste is turned into incineration fly ash during the incineration process. In 2022, the emissions of fly ash from waste incineration in China exceeded 6 million tons. Fly ash from waste incineration contains a large number of dioxins, soluble salts, alkali, and potentially toxic elements (Pb, Cd, Cr, etc.), and it is classified as HW18 (hazardous waste No. 18) [5–7]. The disposal of MSWI fly ash is still dominated by landfill at present, and how to achieve the resource utilization of MSWI fly ash remains a pressing problem to be solved [8].

The main components of MSWI fly ash are similar to solid waste such as coal fly ash and slag and mainly consist of  $\text{SiO}_2$ ,  $\text{CaCO}_3$ ,  $\text{Al}_2\text{O}_3$ , and various silicate/aluminate minerals. MSWI fly ash also contains a glass-phase component after high-temperature calcination and cooling [9–11]. Therefore, MSWI fly ash shows a weak hydration activity and can be used as an auxiliary cementing material for cement and concrete [12]. The application of MSWI fly ash in the fields of cement and concrete has been extensively investigated. Polettini explored the changes in the mechanical properties of a waste incinerator bottom slag–ordinary Portland cement system and the leaching characteristics of trace metals in the material [13]. The results implied that the waste incineration ash slag had a certain activity and could be used as a cement admixture. Li et al. investigated the mechanical properties, hydration mechanism, and leaching toxicity of hardened cement paste mixed with MSWI fly ash and incineration residues. The results showed that the active components in the incinerator fly ash were  $\text{CaO}$ ,  $\text{Al}_2\text{O}_3$ , and  $\text{Fe}_2\text{O}_3$ , with an activity ratio of 43.58%, which was twice as high as that of the incineration residue. The addition of the MSWI fly ash delayed the hydration process of the cement and weakened the strength of the cement [14]. Zhang et al. studied the composition of MSWI fly ash and explored the possibility of using MSWI fly ash as an active admixture for cement concrete. The results indicated that MSWI fly ash is mainly composed of clay minerals and has a certain activity. When the addition of MSWI fly ash was not more than 20%, the role of the MSWI fly ash in the cement was similar to that of low-calcium fly ash, but when the addition of the MSWI fly ash was 30%, the late-stage strength growth of the cement was slow [15]. Qi et al. investigated the use of MSWI fly ash as a cement admixture and found that the setting time of the cement gradually extended, the water requirement for a standard consistency increased, and the strength of the cement showed a downward trend with the increase in the addition of incineration ash. MSWI fly ash exhibits hydration activity and is abundant, making it particularly suitable for preparing coal mine backfill materials [16]. In addition, our team found through experimental research that certain trace components in fly ash can undergo chemical reactions to generate bubbles in the alkaline environment of cement clinker, leading to a micro-expansion of the solidified backfill body. This is highly beneficial for the roof connection of the backfill body in the mined-out area of coal mines [17].

Bottom ash and coal gangue are both bulk industrial wastes. Coal gangue is the largest form of solid waste emitted during coal mining and coal washing, accounting for more than 20% of China's total industrial solid waste. Among the solid wastes in power plants, the emission of bottom ash is second only to fly ash, accounting for from 10% to 30% of the total waste volume [17–20]. Furnace bottom ash is not suitable for use as a building material admixture such as cement and concrete because of its low activity, coarse particles, and uneven distribution, and thus it has not been effectively utilized at present [21]. Bottom ash and coal gangue are largely landfilled or stockpiled, occupying resources, releasing harmful gases for a long time, and damaging the ecological environment [22]. Chinese scholars have also conducted many studies examining the application of furnace bottom ash and coal gangue in the field of mine-filling materials. Lu et al. evaluated the effects of mechanical grinding, microwave irradiation, and additives on the activity of bottom ash and characterized the bottom ash and its cementitious samples using laser particle size analysis, X-ray diffraction, and scanning electron microscopy [23]. Zhang et al. prepared coal-gangue-based backfill materials using solid wastes such as coal gangue and low-quality coal fly ash, and they elucidated the mechanism of the influences of different particle size

combinations on the properties of the backfill materials. The results showed that the change in the particle size of the coal gangue played a major role in the material properties, while the change in the particle size of the low-quality coal fly ash and desulfurization gypsum played a secondary role, and there was an optimal particle size combination, that is, the combination of coal gangue particle sizes ranging from 0.075 to 0.106 mm and MSWI fly ash and desulfurized gypsum particle sizes ranging from 0.053 to 0.075 mm could be optimal [24]. Chen et al. studied the effect of compound activation (mechanical–thermal activation and chemical activation) technology on the flexural and compressive strength of coal gangue–cement backfill materials at different ages. The results implied that the calcination temperature of the coal gangue was around 700 °C, and the ratio of the activators (mass fraction) was 5% quicklime, 1% dihydrate gypsum, and 1.5% sodium sulphate, resulting in a high activity of the coal gangue [25].

The amount of coal pressed under buildings, water bodies, and railways in China's coal mines has reached over 10 billion tons [26]. To maximize the recovery of coal resources, it is necessary to address the technical issues of mining coal under these conditions. The backfill mining method can control the movement of the overlying rock layers and protect ground structures, which is one of the important ways in which to realize green mining in coal mines [27,28]. With the development of coal mine cemented backfill technology, the performance of backfill materials has also been significantly improved. However, the backfill mining method cannot be widely promoted, mainly due to the insufficient early strength and high cost of backfill materials [29]. There are many studies on the properties of coal mine backfilling based on fly ash, but there is still not enough research into the properties of mine backfilling based on MSWI fly ash. In the present work, MSWI fly ash and coal gangue were used as the main raw materials to prepare coal mine backfill materials, which can be used for coal mine backfill mining, reducing the cost of backfill mining, recycling large amounts of solid waste, and protecting the environment.

## 2. Materials and Methods

### 2.1. Materials

The backfill material prepared in this study was a mixture of municipal solid waste incineration (MSWI) fly ash, furnace bottom ash, coal gangue, cementitious material, and water in a certain proportion. The water–cement ratio was determined as 0.37. The specimens were labelled PB1–PB4 and DZ1–DZ3, corresponding to their different raw material components. The coal gangue was sampled from the Lu Gou Coal Mine in Henan Province, China, and it was composed of sandstone and limestone, the sandstone accounting for 32% and the limestone accounting for 68%; the MSWI fly ash was sampled from an MSWI plant in Henan Province, China. It was a yellow-brown powder passing a 100 mesh, and it was formed by the incineration of domestic waste at 850 °C. The MSWI fly ash was dried to constant weight at 105 °C and then ground to 350–380 m<sup>2</sup> kg<sup>−1</sup> to improve the hydration reactivity of the MSWI fly ash. The mineral and chemical compositions of the MSWI fly ash are shown in Figure 1 and Table 1. The primary components in the fly ash were CaO and SiO<sub>2</sub>, which were present in calcite and quartz minerals, respectively. There were also metallic Al and aluminum nitride (AlN) in the form of elementary substances in the fly ash. The furnace bottom ash was sampled from Dongfeng Power Plant in Henan Province, China. It had an irregular grain appearance and was grayish-green or brown in color. Its main component was SiO<sub>2</sub>, which was found in quartz. The reference cement used was P·I 42.5 Portland cement consisting of 95% cement clinker and 5% gypsum, which conformed to the Chinese national standard GB 175-2007 [30]. The quality of the water should conform to the Chinese national standard GB/T 19923-2005 (the reuse of urban recycling water—water quality standard for industrial uses) [31].

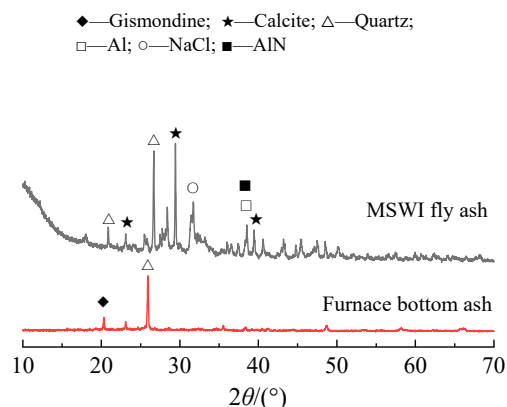


**Figure 1.** XRD spectra of the raw materials.

**Table 1.** Chemical composition of raw materials (% by mass).

Raw Material/Oxide	SiO <sub>2</sub>	Al <sub>2</sub> O <sub>3</sub>	CaO	Fe <sub>2</sub> O <sub>3</sub>	MgO	K <sub>2</sub> O	Na <sub>2</sub> O	TiO <sub>2</sub>	LOI
MSWI fly ash	71.25	15.68	6.62	3.12	0.02	1.56	0.96	0.43	9.71
Furnace bottom ash	51.30	24.55	10.24	5.76	0.87	2.44	0.35	1.55	7.5

## 2.2. Paste Performance and Micro-Testing

The coal gangue was crushed and sieved to a particle size of less than 10 mm. It was mixed with the MSWI fly ash, furnace bottom ash, and standard cement, with water being added to prepare a cementitious paste. The paste was determined using a  $50 \times 150 \times 100 \text{ mm}^3$  CA mortar spread tester according to the Chinese national standard GB50119-2013 “Code for concrete admixture application” [32]. The bleeding rate and initial setting time of the paste were determined according to the Chinese national standard GB/T50080-2016 “Standard for test method of performance on ordinary fresh concrete” [33]. The cementitious paste was injected into a  $40 \times 40 \times 40 \text{ mm}^3$  test mold to produce a solidified sample, and the backfill paste was injected into a  $70.7 \times 70.7 \times 70.7 \text{ mm}^3$  test mold to produce a backfill sample according to the design recipe. The compressive strength of the backfill sample was measured after curing at  $20 \pm 1 \text{ }^\circ\text{C}$  and at 90% humidity for 1 day, 3 days, and 28 days, respectively. The results showed that during the preliminary trial assembly test, the cementitious paste had expansibility during the solidification process; therefore, the rate of expansion was used as a performance indicator. The height of the paste was recorded as  $L_1$  when it was just poured into the mold, and the height of the paste was recorded as  $L_2$  after curing for 12 h, and then the rate of expansion was given by  $(L_2 - L_1)/L_1$ . The cementitious sample cured for 28 days was crushed and screened using a 9.5 mm square-aperture sieve. The leaching tests of the fly ash and solidified sample were conducted using a mixed solution of sulfuric acid and nitric acid with a pH of 3.2 according to the Chinese industry standard HJ/T 299-2007 “Solid waste-extraction procedure for leaching toxicity-sulfuric acid & nitric acid method” [34]. The heavy metal concentration in the leaching solution was determined using inductively coupled plasma mass spectrometry. The contents of dioxins in the fly ash and solidified samples were determined according to HJ 77.4-2008 “Soil and sediment determination of polychlorinated dibenzo-p-dioxins (PCDDs) and polychlorinated dibenzofurans (PCDFs) by isotope dilution HRGC-HRMS” [35].

The oxide compositions of the raw materials were determined using X-ray fluorescence (S8 Tiger XRF, bruker, Karlsruhe, Germany) (Table 1). The mineral composition of the specimens was obtained using an X-ray diffractometer (Rigaku SmartLab, Tokyo, Japan). The experiments were conducted using Cu K $\alpha$  radiation at 40 kV and 30 mA at a scanning speed of  $0.02 \text{ s}^{-1}$  over a scanning range of  $15^\circ$ – $60^\circ$ . The micromorphology of the hydration products was determined using a scanning electron microscope (FEI Quanta 250, Waltham, MA, USA) using an accelerating voltage of 15 kV and an EDAX spectrometer. The

distribution of heavy metal elements in the backfill body was measured using a Jxa8800r electron probe micro-analyzer (Jeol, Tokyo, Japan).

### 3. Results and Discussion

#### 3.1. Effect of the Proportion of Cementitious Materials on Their Working Performance

The experimental design and the results of the effect of the raw material ratio on the strength of the cementitious system are summarized in Table 2. The cementitious component of the backfill material was composed of MSWI fly ash, furnace bottom ash, and reference cement. The water–cement ratio was determined to be 0.37. The samples were labelled PB1–PB4 and DZ1–DZ3, corresponding to their different raw material components. The experimental design and the results of the effect of the raw material ratio on the strength of the cementitious system are shown in Table 2. The strength, especially the early strength of the samples, was found to be greatly reduced compared with the pure cement sample after the fly ash and furnace bottom ash were mixed with the cement. For example, the 3-day strength of the DZ1 group sample was only 34.4% of that of the pure cement sample; this may be attributed to the addition of the fly ash, which caused the sample to expand, resulting in a loose structure and a decrease in strength. Furthermore, the fly ash and bottom ash had lower activities and slower hydration reactions compared to the cement clinker and thus resulted in a lower early strength.

**Table 2.** Effect of the sludge ash content on mechanical properties of the cementitious system.

Sample	Raw Material Content (%)			Expansion Rate (%)	Compressive Strength (MPa)		
	Fly Ash	Furnace Bottom Ash	Reference Cement		–	3 d	7 d
PB1	25	25	50	7.2	13.4	19.3	28.9
PB2	35	15	50	10.8	11.9	17.1	27.7
PB3	35	35	30	6.5	9.4	15.2	25.4
PB4	50	20	30	9.1	8.1	12.9	24.0
DZ1	50	0	50	12.7	6.6	11.4	19.1
DZ2	0	50	50	0	15.6	21.5	31.8
Pure cement	0	0	100	0	19.2	30.9	43.7

Comparing the results of the PB1, PB2, and DZ1 groups shown in the table, the rate of expansion of the cementitious system continued to increase, and the compressive strength at each age decreased with increasing amounts of MSWI fly ash under the same cement content [36]. For example, the rate of expansion of DZ1 was 76.4% higher than that of PB1; nevertheless, the compressive strength of the DZ1 group was only 49.3% of that of PB1 after curing for three days. The expansion of the cementitious pastes might be attributed to the foaming reaction of the MSWI fly ash with the alkaline solution in the cementitious pastes, and the increase in the rate of expansion may be due to the increased mixing ratio of fly ash, resulting in a more violent foaming reaction. Comparing the results of DZ1 and DZ2, the increase in the amount of furnace bottom ash was beneficial to the improvement of the samples' strength [37]. This may be attributed to the fact that the furnace bottom ash contained more active components that participated in the alkali-activated reaction in the alkaline solution of the cement, forming more hydrated products and thus enhancing the strength of the sample. Comparing PB1 and PB3, the rate of expansion of PB3 was still lower than that of PB1 despite the increase in fly ash addition; this may be due to the lower cement content in PB3 and the insufficient alkalinity of the paste, resulting in fewer bubbles produced by the fly ash foaming reaction.

#### 3.2. Effects of Admixtures on the Properties of the Cementitious Materials

To improve the expansion performance of the backfill material, this research attempted to add a small amount of NaOH to improve the alkalinity of the slurry and CaCl<sub>2</sub> to enhance the early strength of the cementitious material [37–39]. The raw material ratio was based

on the PB1 formula with the addition of admixtures. The experimental design and results are summarized in Table 3. It can be seen that the addition of NaOH was beneficial to the improvement of the expansion properties of the cementitious materials. When the NaOH content was 0.9%, the rate of expansion of the paste increased by 120.8% compared to that of the PB1 group, but the strength of PZ3 decreased significantly, which was only 53.7% of that of specimens in the PB1 group at three days. This may be attributed to the increase in the alkalinity of the paste solution caused by the addition of the NaOH, which intensified the foaming reaction and produced more bubbles, causing an increase in the specimen volume but also a decrease in the density and compressive strength. Therefore, the content of NaOH added in the paste should not be too much.  $\text{CaCl}_2$  could slightly increase the rate of expansion of the paste. When the addition of  $\text{CaCl}_2$  was 1.8%, the rate of expansion of ZQ6 was 40.3% higher than that of the PB1 group. This may be due to the fact that the  $\text{CaCl}_2$  promoted the hydration of the cement clinker and formed more alkaline hydration products, which aggravated the foaming reaction of the fly ash [40].

**Table 3.** Effect of the admixture on properties of the cementitious material.

Specimen	Admixture	Admixture Mass Fraction (%)	Compressive Strength (MPa)			Expansion Rate (%)
			3 d	7 d	28 d	
PB1	–	–	13.4	19.3	28.9	7.2
PZ1	NaOH	0.3	11.3	16.6	23.1	10.6
PZ2		0.6	9.7	12.8	21.5	13.7
PZ3		0.9	7.2	11.6	20.4	15.9
ZQ4	$\text{CaCl}_2$	0.8	15.2	20.4	29.3	7.5
ZQ5		1.3	17.7	23.0	30.8	9.0
ZQ6		1.8	18.2	25.7	31.2	10.1

The compressive strength of the specimens increased significantly after adding the  $\text{CaCl}_2$ . The strength of ZQ6 cured for 3, 7, and 28 days increased by 35.8%, 33.2%, and 8% compared to PB1, respectively; among them, the 3-day strength increased the most, indicating that the  $\text{CaCl}_2$  mainly acted at the early hydration stage. The addition of  $\text{CaCl}_2$  could compensate for the reduction in strength caused by the foaming and expansion of the paste to a certain extent. This could help the backfill material to resist the deformation of the working face caused by mining-induced pressure.

### 3.3. XRD Analysis of Hydration Products

Figure 2a,b illustrate the XRD analysis spectra of the backfill cementitious materials after curing for three days and twenty-eight days. As shown in Figure 2a, the main hydration products of the cementitious material were hydrated calcium chloroaluminate ( $3\text{CaO}\cdot\text{Al}_2\text{O}_3\cdot\text{CaCl}_2\cdot 10\text{H}_2\text{O}$ ), portlandite ( $\text{Ca}(\text{OH})_2$ ), and crystalline C-A-S-H (hydrated calcium aluminosilicate), as well as minerals containing potentially harmful elements, i.e., calcium zinc aluminum oxide ( $\text{Ca}_3\text{Al}_4\text{ZnO}_{10}$ ) and laurionite [ $\text{Pb}(\text{OHCl})$ ] [41–43]. Quartz and calcite were present in the unhydrated fly ash, and dicalcium silicate was present in the unhydrated cement. Portlandite and C-S-H are mainly formed by the hydration of calcium silicate in cement clinker, and the amount of portlandite can usually reflect the degree of hydration of cement clinker. A hydrated calcium aluminate chloride and C-A-S-H gel may be formed by the co-reaction of Al, AlN, NaCl, KCl, and the hydration product  $\text{Ca}(\text{OH})_2$  in the raw material of MSWI fly ash. The results further proved that the foaming reaction of the cementitious materials involved the interaction of Al and AlN with alkali solutions [44]. A diffuse peak appeared at a  $2\theta$  of  $31^\circ\sim 35^\circ$ , indicating that a large amount of hydrated calcium (aluminum) silicate gel was generated. Comparing the PZ3 and ZQ6 results shown in Figure 3b, the diffraction peaks of hydrated calcium chloroaluminate were enhanced significantly upon NaOH doping, indicating an increase in the production of hydrated calcium aluminate, which was attributed to the fact that the

Al and AlN in the raw materials of the MSWI fly ash formed a layer of dense, solid  $Al_2O_3$  and  $Al(OH)_2$  film in the air, and the film was dissolved by the NaOH solution; furthermore, the Al and AlN could react with water to form hydrogen, ammonia, and hydrated calcium chloroaluminate, which was the reason for the higher rate of expansion of W2. Compared with PB1 and ZQ6, the addition of  $CaCl_2$  enhanced the diffraction peaks of portlandite and hydrated calcium chloroaluminate, while the diffraction peaks of dicalcium silicate decreased in amplitude, which could be due to the fact that the  $CaCl_2$  promoted the hydration reaction of the fly ash–furnace bottom ash–cement cementitious system to produce more alkaline  $Ca(OH)_2$ , which reacted with the Al and AlN in the fly ash to produce the hydrated calcium chloroaluminate [45]. This is also the reason why  $CaCl_2$  can improve the material rate of expansion. Comparing Figure 3a,b, the diffraction peak of dicalcium silicate and quartz decreased in amplitude with the extension of the curing age, the diffraction peak of portlandite enhanced, and the production increased. This finding suggested that the more reactive  $SiO_2$  and  $Al_2O_3$  in the fly ash were involved in the alkali excitation reaction.

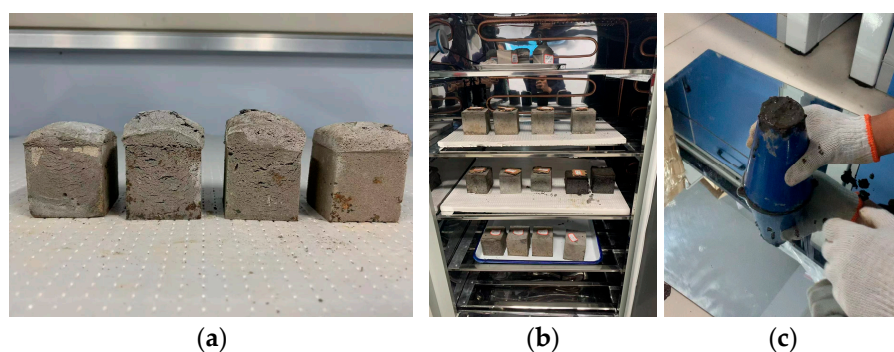


Figure 2. Preparation of test specimens: (a) specimen of cementitious materials; (b) specimen of backfill materials; (c) slump tests.

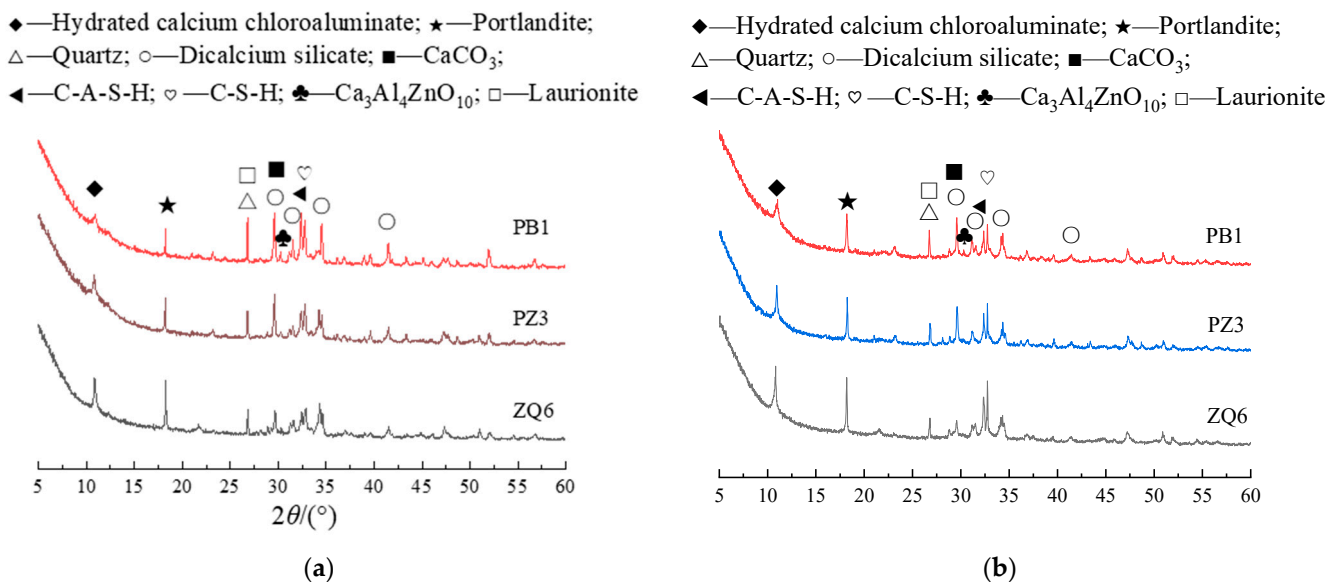
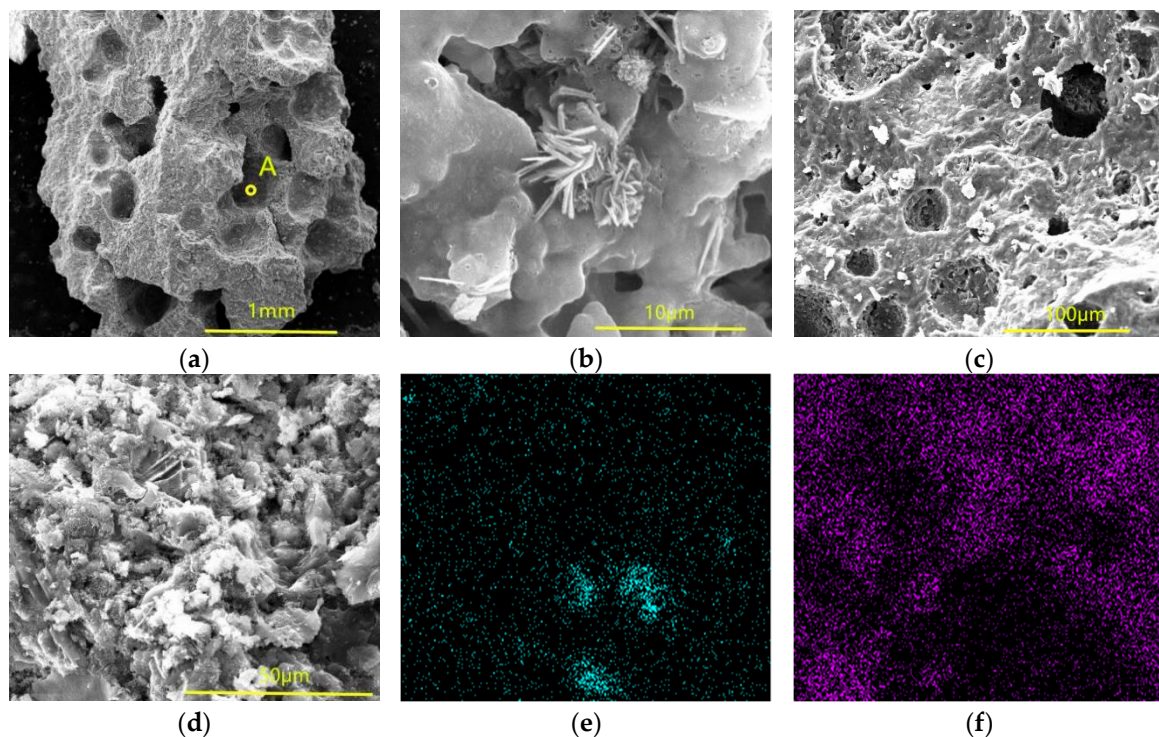


Figure 3. XRD analysis spectra of the backfill cementitious materials after curing for three days and twenty-eight days: (a) XRD analysis spectrum of backfill material after three days of solidification; (b) XRD analysis spectrum of backfill material after twenty-eight days of solidification.

### 3.4. SEM Analysis of Hydration Products

Figure 4 shows the SEM images and electron probe backscattering images of the PZ3 and ZQ6 specimens. Figure 4a demonstrates that the fly ash–furnace bottom ash–cement cementitious system produced more air holes with a pore diameter of 0.1–0.5 mm after

the addition of the NaOH, and the air holes were inter-connected, leading to a decrease in intensity. There were petal-shaped crystals in the A region inside the pore wall of the PZ3 sample (Figure 4b), which were determined to be hydrated calcium chloroaluminate based on the hexagonal lamellar morphology of the crystals [46], proving once again that the MSWI fly ash was involved in the hydration reaction. Figure 4d shows the microscopic morphology of the ZQ6 sample. The porosity of the sample was smaller than that of the PZ3 sample, and the pore diameter ranged between 0.02 and 0.1 mm. There was a dense gel structure between the pores, which led to a high macro strength of the sample. This was because the  $\text{CaCl}_2$  could promote the hydration reaction of the fly ash–furnace bottom ash–cement cementitious system, forming a dense microstructure. Figure 4d depicts the microstructure of the PZ3 sample after 28 days of hydration. The microstructure of the PZ3 sample became more compact, and the strength further increased after 28 days of hydration, which was conducive to increasing the compactness and resistance to damage of the backfill body. Figure 4e,f present the distribution diagrams of the Pb and Ni in Figure 3a, respectively. The brighter the image, the greater the concentration of the element. There were many areas with a significantly higher brightness in the imaging maps of Pb and Ni, indicating the enrichment of these two elements in the distribution of the gel material. According to the morphological characteristics shown in Figure 4d, Pb and Ni were solidified in the gel phase of the hydration products, while other heavy metal elements were not enriched, which was more favorable to reducing the leaching of potentially harmful elements in the sample.



**Figure 4.** SEM micrographs and electron probe backscattering images obtained from hydrated samples: (a) SEM micrograph of specimen PZ3 cured for three days; (b) enlarged view of microregion A; (c) SEM micrograph of specimen ZQ6 cured for three days; (d) SEM micrograph of specimen PZ3 cured for twenty-eight days; (e) distribution diagrams of Pb in Figure 2a; (f) distribution diagrams of Ni in Figure 2a.

### 3.5. Determination of the Optimal Particle Size Distribution of Coal Gangue

Particle gradation refers to mixing different sizes of aggregates in a certain proportion to achieve a relatively dense state. Particle gradation exerts a significant influence on the strength of backfill material, so it is necessary to determine the optimal particle gradation

through experiments. Fractal theory includes the principles of self-similarity and iterative generation. The composition characteristics of the particle gradation can be obtained using the fractal dimension, and a reasonable relationship between the fractal dimension and the strength of the backfill material can be established; the optimal particle gradation scheme can then be determined using the fractal dimension.

The particle size distribution function is first defined to represent the fractal dimension of the particle size distribution of backfill aggregates:

$$F(x) = \frac{N(x)}{N_0} \quad (1)$$

$N(x)$ —The number of aggregates with a particle size not bigger than  $x$ ;

$N_0$ —The total number of aggregates.

According to the definition of a fractal  $N \propto \delta^{-D}$ , the dimensionless components  $\frac{x}{x_{max}}$  are constructed. Considering the case when  $x = x_{max}$ ,  $N(x_{max}) = N_0$  is established, the total number of aggregates with a particle size not greater than sieve size  $x$  is:

$$N(x) = N_0 \left( \frac{x}{x_{max}} \right)^{-D} \quad (2)$$

Thus, the particle size distribution function can be obtained as:

$$F(x) = \left( \frac{x}{x_{max}} \right)^{-D} \quad (3)$$

After a series of derivations (omitted in this article), the particle size distribution quality distribution function can be determined as:

$$P(x) = \frac{x^{-(D-3)} - x_{min}^{-(D-3)}}{x_{max}^{-(D-3)} - x_{min}^{-(D-3)}} \quad (4)$$

Neglecting  $X_{min}$  due to the very small size of the backfill aggregate, the following can be derived:

$$P(x) = \frac{M(x)}{M_0} = \left( \frac{x}{x_{max}} \right)^{3-D} \quad (5)$$

It can be seen from Equation (5) that the mass distribution of aggregate particle gradation can be established as a relationship with the fractal dimension  $D$ . The value range of the fractal dimension of the aggregate is between the topological dimension and the spatial dimension through the analysis of the concept of fractal dimension, that is,  $2 < D < 3$ . Taking logarithms on both sides of Equation (5), we obtain:

$$\lg \frac{M(x)}{M_0} = (3 - D) \lg(x) + b \quad (6)$$

$b$  is a constant, and taking  $\lg \frac{M(x)}{M_0}$  as the ordinate and  $\lg x$  as the abscissa, the data pertaining to the quality distribution of the particle size grading of the aggregate can be fitted into a straight line; let  $k = 3 - D$ , where  $k$  is the slope of the line, whence the fractal dimension is denoted by  $D$ .

To achieve the pressure pumping of the backfill slurry, it was ensured that the pipe was not blocked, the strength of the backfill body was ensured, and the coal gangue was crushed and screened to a maximum particle size of 4.75 mm and 9.5 mm, respectively. The aggregate grading design and screening results are listed in Table 4.

**Table 4.** Results of aggregate gradation.

Number	Percentage Passing (%)							
	0.075	0.15	0.3	0.6	1.18	2.36	4.75	9.5
S1	6.24	14.59	25.42	34.27	49.30	78.11	100	0
S2	5.61	12.87	21.33	32.18	47.35	75.99	100	0
S3	3.82	9.55	17.26	26.19	39.93	73.07	100	0
S4	4.87	12.33	22.01	31.15	41.43	63.76	88.29	100
S5	3.23	10.68	18.59	26.11	35.60	60.44	85.10	100
S6	1.71	7.78	15.86	22.70	30.31	54.47	80.54	100

According to Equation (6), the aggregate screening results were imported into a double logarithmic coordinate system, and the Curve Fitting Tool in MATLAB™ R2018a software was used to fit the aforementioned data using the least squares method. The fractal dimension  $D$  of the particle size distribution was calculated. The results are summarized in Table 5.

**Table 5.** The fitting result and fractal dimension of the aggregate particle distribution.

Number	Fitting Equation	Correlation Coefficient ( $R^2$ )	Grain Size Distribution Fractal Dimension ( $D$ )
S1	$y = 0.6x + 1.64$	0.9669	2.4
S2	$y = 0.7x + 1.62$	0.9779	2.3
S3	$y = 0.8x + 1.55$	0.9802	2.2
S4	$y = 0.6x + 1.54$	0.9479	2.4
S5	$y = 0.7x + 1.49$	0.9400	2.3
S6	$y = 0.8x + 1.41$	0.9207	2.2

To establish the relationship between the fractal dimension of the particle size distribution and the strength of the backfill body, a single-factor test method was used to conduct strength experiments on the backfill material. The backfill cementitious material consisted of MSWI fly ash, furnace bottom ash, and reference cement, with mixing ratios of 35%, 15%, and 50%, respectively, and a  $\text{CaCl}_2$  addition of 1.3%. To increase the fluidity of the paste, a 1.5% content of a naphthalene-based water reducer was added, and the ratio of cementitious material to coal gangue was 1:4. The mass concentration calculation formula for the backfill material was  $(m_{(\text{cementitious material})} + m_{(\text{coal gangue})}) / (m_{(\text{cementitious material})} + m_{(\text{coal gangue})} + m_{(\text{water})})$ , and the mass concentration was set to 79%. The compressive strength test was conducted, and the results are listed in Table 6.

**Table 6.** Compressive strengths of the backfill body with different particle size distributions.

Number	Fractal Dimension	Compressive Strength (MPa)		
		1 d	3 d	28 d
S1	2.4	0.72	1.43	3.26
S2	2.3	0.60	1.31	3.11
S3	2.2	0.55	1.15	2.62
S4	2.4	0.64	1.33	2.92
S5	2.3	0.58	1.12	2.53
S6	2.2	0.52	1.07	2.37

As presented in Table 6, the compressive strengths of the six groups of mixed aggregates increased with increasing the fractal dimension. Among the three groups of specimens with a maximum particle size of 4.75 mm, the compressive strengths of the group S1 samples cured for 1 day, 3 days, and 28 days were 30.9%, 24.3%, and 24.4% higher than those of group S3, respectively; among the three groups of specimens with

a maximum particle size of 9.5 mm, the compressive strengths of the group S4 samples cured for 1 day, 3 days, and 28 days were 23.1%, 24.3%, and 23.2% higher than those of group S6, respectively. The number of fine particles in the mixed aggregate increased as the fractal dimension decreased based on the screening results in Table 4. The fine particles of aggregate filled the interstices between the coarse particles, resulting in an increased density and strength of the backfill body.

Table 6 shows that when the fractal dimension values were the same, the strength of the specimens with a maximum grain size of 4.75 mm at each age was higher than that of the specimens with a maximum grain size of 9.5 mm. This was attributed to the fact that the content of fine particles in the mixed aggregate increased as the maximum particle size of the aggregate decreased. The contact area between the aggregate and the cementitious paste increased, thus enhancing the cohesion between the cementitious paste and the aggregate, further improving the strength of the backfill body. In summary, the S1 gradation was the best among the six particle size gradation schemes, and the strength of the backfill body prepared therewith was the highest.

### 3.6. Effects of the Mass Concentration on the Working Performance of Backfill Materials

The experimental design was conducted according to the single-factor test method. The backfill cementitious material was composed of MSWI fly ash, furnace bottom ash, and reference cement. The contents of these components were 35%, 15%, and 50%, respectively. The content of CaCl<sub>2</sub> was 1.3%. The content of naphthalene-based water reducer was 1.5%, the ratio of cementitious material to coal gangue was 1:4, and the particle size distribution followed the S1 mixing ratio scheme. The mass concentrations of the backfill material were set to 78%, 78.5%, 79%, 79.5%, 80%, and 80.5%, and the effects of the mass concentration on the slump, bleeding rate, rate of expansion, and compressive strength of the backfill material were determined.

Table 7 shows that the slump decreased as the concentration of the backfill paste increased. The slump of the W6 specimen was only 83 mm, making it difficult to transport over long distances and therefore not suitable for engineering applications. The water-bleeding rate of the paste decreased as the concentration of the slurry increased. For example, the water-bleeding rates of the W1 and W2 groups with concentrations of 78% and 78.5%, respectively, reached 7.2% and 4.5%, exceeding the limit of 3%; therefore, they were not adopted in practice. The segregation of coarse aggregates during transportation will be caused by a high water-bleeding rate, causing blockage of the conveying pipeline, and excess backfill water could contaminate the roadway and increase drainage costs. Therefore, it is recommended to choose a mass concentration between 78.5% and 80%.

**Table 7.** Effects of the mass concentration on the working performance of backfill materials.

Number	Mass Concentration (%)	Slump (mm)	Bleeding Rate (%)	Expansion Rate (%)	Compressive Strength (MPa)		
					1 d	3 d	28 d
W1	78	141	5.2	13.6	0.32	0.94	1.87
W2	78.5	135	2.9	12.1	0.54	1.21	2.50
W3	79	132	2.7	10.9	0.72	1.43	3.26
W4	79.5	123	2.3	8.8	0.82	1.51	3.31
W5	80	111	2.1	6.7	0.97	1.74	3.52
W6	80.5	83	1.8	4.2	1.16	2.13	3.68

The compressive strength of the consolidated body at every age continued to increase with the increasing concentration of the paste. When the concentration increased from 79.5% to 80%, the strength at the three ages increased by 18.3%, 15.2%, and 6.3%, respectively. The rate of expansion of the consolidated bodies decreased as the concentration increased, and all were smaller than the specimens containing pure cementitious material, which may be due to the diluting effect of the aggregate. The W3, W4, and W5 samples

could all meet the design requirements for the various properties of consolidated bodies in backfill mining, and they can be considered as being of the preferred ratio.

### 3.7. Effects of Cementitious Material Addition on the Working Performance of Backfill Materials

The backfill cementitious material was composed of MSWI fly ash, furnace bottom ash, and benchmark cement. The contents of these components were 35%, 15%, and 50%, respectively. The content of  $\text{CaCl}_2$  was 1.3%. The content of naphthalene-based water reducer was 1.5%, and the particle size distribution followed the S1 mixing ratio scheme; the mass concentration of the paste was 79%, and the contents of the cementitious material were set to 10%, 15%, 20%, 25%, and 30%, giving five groups, numbered from C1 to C5. The test results are summarized in Table 8.

**Table 8.** The effect of the cementitious material addition on the working performance of backfill materials.

Number	Content of Cementitious Materials (%)	Slump (mm)	Bleeding Rate (%)	Setting Time (min)	Compressive Strength (MPa)		
					1 d	3 d	28 d
C1	10	131	3.4	375	-	0.28	0.83
C2	15	134	2.9	285	0.31	0.96	1.75
C3	20	137	2.7	245	0.72	1.43	3.26
C4	25	138	2.4	220	1.12	2.28	5.51
C5	30	140	1.8	205	1.82	3.08	8.33

Table 8 indicates that the compressive strength of the consolidated body increased with the increase in the amount of cementitious material. When the amount of cementitious material was 10%, the test block was too soft to measure the strength value. The strength of the specimens cured for 28 d was only 0.83 MPa, which usually cannot meet the later strength requirements of backfill material. Therefore, the 10% addition scheme was not adopted. When the amount of cementitious material was 20%, 25%, and 30%, the corresponding 1-day and 28-day strengths exceeded 0.7 MPa and 3 MPa, respectively. Generally, this can meet the strength requirements in the early and late stages. It is reasonable to choose the 20% and 25% addition schemes, considering the cost of the backfill. The slump of the slurry tended to increase as the addition of cementitious materials increased, but the growth rate therein was relatively small, with an increase in slump of only 9 mm from 10% to 30% of the amount added. The increase in the slump of the paste may be due to the lubricating and rolling effects of the fine particle powders in the cementitious material on the backfill paste.

The water-bleeding rate of the backfill paste gradually decreased as the amount of cementitious material increased. When the amount of cementitious material was 30%, the water-bleeding rate reached the lowest level of 1.8%. The decrease in the water-bleeding rate may be due to the increase in fine particles in the paste, which formed a network of condensed spatial structures through water film interconnection under the action of the molecules. This reduced the formation of capillary pathways and pores within the backfill material, thereby decreasing the water-bleeding rate. The setting time of the slurry decreased as the amount of cementitious material increased due to the increase in the number of active components in the cementitious material, which accelerated the hydration reaction of the backfill material and reduced the setting time of the paste.

### 3.8. Heavy Metal Leaching and Dioxin Concentration

Table 9 shows the leaching concentrations of the four potentially harmful elements, with higher contents in the raw materials and hydration products. As presented in Table 9, Ni, Pb, Cd, and As elements in the MSWI fly ash were all higher than the limits set out in the Chinese national standard GB 5085.7-2019 "Identification standards for hazardous waste: general rules" [47]. The leaching concentration of potentially harmful elements was greatly reduced after preparing the fly ash as a backfill material, and all of them were lower than

the leachable heavy metal concentration limit set by the hazardous waste identification standard and the Chinese industry standard HJ 1134-2020 “Technical specification for pollution control of fly-ash from municipal solid waste incineration” and the Chinese industry standard GB 30760-2014 “Technical specification for coprocessing of solid waste in cement kiln” [48,49]. This was due to the dilution effect of the cement on the one hand and, on the other hand, the hydration of the fly ash–furnace bottom ash–cement cementitious system forming C-S-H and C-A-S-H, with its dense structure (Figure 3c) and extremely low permeability, and the heavy metal fixation in the backfill material, which could restrict the migration of the free-state heavy metal ions outward through physical encapsulation. This was also the reason why the leaching of potentially harmful elements from the specimens of the backfill material was relatively low [50]. The alkaline environment formed by the fly ash–furnace bottom ash–cement cementation system promoted the occurrence of a re-decomposition precipitation reaction, thus leading to the formation of very-low-solubility hydroxides of heavy metal ions, such as laurionite [51]; in addition, the  $\text{Ca}^{2+}$  in the hydrated calcium chloroaluminate structure formed by the fly ash–cement cementitious system could fix  $\text{Cd}^{2+}$ ,  $\text{Pb}^{2+}$ ,  $\text{Ni}^{2+}$ , etc., through homocrystalline replacement, thus fixing the potentially harmful elements in the cement structure and decreasing their leaching concentration [52]. The total dioxin concentration in the fly ash raw material was 426 ng-TEQ/kg, and that of the W3, W6, and C5 specimens was 45, 31, and 13 ng-TEQ/kg, respectively, which was lower than the limit value of the dioxin content in fly ash treatment products codified in HJ 1134-2020 “Technical specification for pollution control of fly-ash from municipal solid waste incineration” [48]. The reduction in the concentration of dioxin in the solidified body may have been due to the dilution and encapsulation effects of the cement.

**Table 9.** The heavy metal leaching concentration of fly ash and cementitious materials.

Element	Concentration of Heavy Metal Ions in the Leaching Solution (mg/L)					
	Leaching Solution of fly Ash Raw Materials	W3 Leaching Solution	W6 Leaching Solution	C5 Leaching Solution	GB 5085.3-2007 Limit Values of Hazardous Waste Identification Standards [53]	GB 30760-2014 Limits for the Leachable Heavy Metal Concentrations in Cement Clinker
Ni	8.53	0.18	0.11	0.03	5	0.2
Pb	32.45	0.26	0.19	0.09	5	0.3
Cd	4.86	0.02	0.01	ND	1	0.03
As	7.34	0.07	0.02	ND	5	0.1

#### 4. Conclusions

- (1) The rate of expansion of the cementitious system continued to increase and the compressive strength decreased as the mass ratio of MSWI fly ash to furnace bottom ash increased. Aluminum and aluminum nitride in the fly ash reacted with water to generate gases, causing an expansion of the cementitious material. The sodium hydroxide increased the alkalinity of the solution, promoting the formation of more bubbles, thereby improving the expansion properties of the cementitious material. Its maximum rate of expansion could reach 15.9%. The addition of calcium chloride promoted the early hydration reaction of the cementitious materials, forming a dense microstructure and enhancing the early strength and rate of expansion of the cementitious materials. Both lead and nickel were solidified in the gel phase of the hydration products, which was more favorable to reducing the leaching of potentially harmful elements from the specimens.
- (2) The compressive strength of the backfill body continued to increase with the increasing fractal dimension of aggregate particles. The compressive strength of the backfill body increased as the maximum particle size of the aggregate decreased when their fractal dimensions were the same. Among the six particle size gradation schemes, the S1 gradation scheme was optimal, with the strength of the prepared backfill body reaching 0.72 MPa, 1.43 MPa, and 3.26 MPa at 1 day, 3 days, and 28 days, respectively.

- (3) As the concentration of the backfill paste increased, the slump, water-bleeding rate, and consolidation and rate of expansion of the paste continuously decreased, while the compressive strength of the consolidated body at various ages continuously increased (the higher the concentration of the paste, the larger the increase in the compressive strength), and the specimens from the W3, W4, and W5 groups could all meet the design requirements for material properties in backfill mining, and they could be used as the preferred ratio. The compressive strength of the backfill body and the slump of the paste increased with the increase in the amount of cementitious material. The water-bleeding rate of the backfill paste gradually decreased, and the setting time of the paste was decreased.
- (4) After the MSWI fly ash was prepared as the backfill material, the leaching of nickel, lead, cadmium, and arsenic elements in the fly ash could be greatly reduced, and the concentration of dioxin was reduced to 13 ng TEQ/kg. This result was attributed to the dilution of the cement, the physical encapsulation of the gel products, and the isomorphous replacement of  $\text{Ca}^{2+}$  in the calcium aluminate chloride hydrate.

**Author Contributions:** Conceptualization, Z.W. and H.L.; methodology, Z.C.; software, Y.J.; validation, G.L., R.Z. and Y.Z.; formal analysis, Z.C.; investigation, Y.Z.; resources, M.Y.; data curation, Z.W.; writing—original draft preparation, Z.W.; writing—review and editing, Z.W.; visualization, H.L.; supervision, H.L.; project administration, Z.W.; funding acquisition, Z.W. All authors have read and agreed to the published version of the manuscript.

**Funding:** This research was funded by the Natural Science Foundation of Xinjiang Uygur Autonomous Region, grant number 2022D01A116; the Key R&D Special Funds Project of Xinjiang Uygur Autonomous Region, grant number 2022B01034 and 2023B01010; and the Science and Technology Research Project of Henan Province, grant number 232102320113.

**Data Availability Statement:** The research data used to support the findings of this study are currently under embargo while the research findings are commercialized. Requests for data, 12 months after publication of this article, will be considered by the corresponding author.

**Conflicts of Interest:** Zhen Wang, Zhiwen Chen, Yongyong Jia, Mingchao Yong are employees of Institute of Coal Science. The paper reflects the views of the scientists and not the company.

## References

1. Zhang, D.S.; Wang, J.; Yue, Z.B.; Wu, J.X.; Yang, Y.H. Experimental study on preparation of lightweight low-silicon-aluminum ceramsite from municipal solid waste incineration fly ash in conjunction with bottom ash. *Environ. Pollut. Control* **2024**, *46*, 32–37.
2. Cao, W.; Wang, Z.H.; Huang, J.N.; Wu, B.S.; Tai, J.; Zhao, J.; Qian, G.R. Disposal pattern of municipal solid waste and influencing factors: Based on data of 134 countries. *Acta Sci. Circumstantiae* **2020**, *40*, 3062–3070.
3. Li, Q.Q.; Ran, G.Z.; Zhang, P. Analysis on the status and trend of domestic waste incineration fly ash disposal in China. *China Resour. Compr. Util.* **2023**, *41*, 99–102.
4. Levent, B.; Yusuf, A.Ç.; Mustafa, S. Analysis of the effects of domestic waste disposal methods on mucilage with life cycle assessment. *Mar. Pollut. Bull.* **2022**, *180*, 113813.
5. Mab, B.; Yang, H.; Wang, Y.F. Overview of resources reuse technologies and corresponding products for municipal solid waste incineration fly ash. *Environ. Chem.* **2023**, *42*, 2669–2687.
6. Peng, Z.; Weber, R.; Ren, Y.; Wang, J.; Sun, Y.; Wang, L. Characterization of PCDD/Fs and heavy metal distribution from municipal solid waste incinerator fly ash sintering process. *Waste Manag.* **2020**, *103*, 260–267. [[CrossRef](#)] [[PubMed](#)]
7. He, P.J.; Wu, C.L.; Zhang, H.; Liu, X.; Shao, L.M. The long-term leaching behavior of air pollution control residues and its treatment products. *Environ. Chem.* **2008**, *27*, 786–790.
8. Trindade, A.B.; Palacio JC, E.; González, A.M.; Orozco DJ, R.; Lora EE, S.; Renó, M.L.G.; del Olmo, O.A. Advanced exergy analysis and environmental assesment of the steam cycle of an incineration system of municipal solid waste with energy recovery. *Energy Convers. Manag.* **2018**, *157*, 195–214. [[CrossRef](#)]
9. Wu, H.; Liu, H.; Tian, S.; Lu, G.; Hao, Y. Current situation for utilization and disposal and environmental management of fly ash from municipal solid waste incineration. *J. Environ. Eng. Technol.* **2021**, *11*, 1034–1040.
10. Jiao, F.; Zhang, L.; Dong, Z.; Namioka, T.; Yamada, N.; Ninomiya, Y. Study on the s pecie s of heavy metals in MSW incine ration fly as h and their leaching be havior. *Fuel Process. Technol.* **2016**, *152*, 108–115. [[CrossRef](#)]
11. Darmansyah, D.; You, S.J.; Wang, Y.F. Advancements of coal fly ash and its prospective implications for sustainable materials in Southeast Asian countries: A review. *Renew. Sustain. Energy Rev.* **2023**, *188*, 113895. [[CrossRef](#)]

12. Tian, Y.; Bourtsalas, A.T.; Kawashima, S.; Themelis, N.J. Using Waste-to-Energy Fine-Combined Ash as Sand or Cement Substitute in Cement Mortar. *J. Mater. Civ. Eng.* **2023**, *35*, 04023378. [[CrossRef](#)]
13. Polettini, A.; Pomi, R.; Fortuna, E. Chemical activation in view of MSWI bottom ash recycling in cement-based systems. *J. Hazard. Mater.* **2009**, *162*, 1292–1299. [[CrossRef](#)] [[PubMed](#)]
14. Li, X.; Yu, Z.; Ma, B.; Wu, B. Effect of MSWI fly ash and incineration residues on cement performances. *J. Wuhan Univ. Technol. Mater.* **2010**, *25*, 312–315. [[CrossRef](#)]
15. Zhang, W.S.; Sui, T.B.; Yao, Y. Study on properties of incinerator ash a cement admixture. *J. Chin. Ceram. Soc.* **2006**, *34*, 229–232.
16. Qi, F.; Gao, F. Research on municipal solid waste incinerator residues as cement admixture. *J. Cem. Eng.* **2009**, *4*, 84–86.
17. Fan, C.; Wang, B.; Ai, H.; Qi, Y.; Liu, Z. A comparative study on solidification/stabilization characteristics of coal fly ash-based geopolymer and Portland cement on heavy metals in MSWI fly ash. *J. Clean. Prod.* **2021**, *319*, 128790. [[CrossRef](#)]
18. Liu, X.W.; Zhao, J.W. Analysis of the current situation of comprehensive utilization of coal gangue. *Inn. Mong. Coal Econ.* **2023**, *41*, 25–27.
19. Joublat, R.A.; Al Basiouni Al Masri, Z.; Absi, J.; ElKordi, A. Investigation of using municipal solid waste incineration fly ash as alternative aggregates replacement in hot mix asphalt. *Road Mater. Pavement Des.* **2023**, *24*, 1290–1309. [[CrossRef](#)]
20. Taha, Y.; Elghali, A.; Derhy, M.; Amrani, M.; Hakkou, R.; Benzaazoua, M. Towards an integrated approach for zero coal mine waste storage: Solutions based on materials circularity and sustainable resource governance. *Miner. Process. Extr. Metall. Rev.* **2023**, *44*, 375–388. [[CrossRef](#)]
21. Ibrahim, N.M.; Mohamed, S.A.; Amat, R.C.; Rahim, N.L.; Zailani, W.W.A.; Rahim, M.A.; Laslo, L.; Ismail, K.N. Viability Study on Fly Ash and Bottom Ash from Combustion Waste. In Proceedings of the IOP Conference Series: Earth and Environmental Science, 4th International Conference on Green Environmental Engineering and Technology (ICONGEET-2022), Seoul, South Korea, 17–18 November 2022; Volume 1216, p. 012025.
22. Spreadbury, C.J.; Weiksnar, K.D.; Laux, S.; Townsend, T.G. Distributions of trace elements within MSWI bottom and combined ash components: Implications for reuse practices. *Chemosphere* **2023**, *336*, 139198. [[CrossRef](#)] [[PubMed](#)]
23. Lu, Q.M.; Zhang, Y.X.; Zhao, J.K.; Li, Y. Experimental study on activation of hydration activity of coal bottom ash in coal-fired power plant. *J. Henan Polytech. Univ. (Nat. Sci. Ed.)* **2021**, *40*, 101–107.
24. Zhang, Q.S.; Li, H.T.; Li, Z.F.; Zhang, J. Influence of different grain size combination on gangue-based filling material. *J. Met. Mine* **2020**, *55*, 73–80.
25. Chen, J.; Shi, Y.; Hu, Q.X. Study on coal gangue activation technology based on filling material in goaf area. *J. Met. Mine* **2013**, *44*, 679–682.
26. Chen, C. Research on the production and design of coal mining in three downs coal mining. *Inn. Mong. Coal Econ.* **2015**, *33*, 28–29.
27. Hu, B.N. Backfill Mining Technology and Development Tendency in China Coal Mine. *Coal Sci. Technol.* **2012**, *40*, 1–5.
28. Zhang, D.D. Application of filling technology of gangue and fly ash in three downs coal mining in Xinyang coal mine. *Energy Energy Conserv.* **2018**, *239*, 120–121.
29. Bazaluk, O.; Petlovanyi, M.; Lozynskiy, V.; Zubko, S.; Sai, K.; Saik, P. Sustainable Underground Iron Ore Mining in Ukraine with Backfilling Worked-Out Area. *Sustainability* **2021**, *13*, 834. [[CrossRef](#)]
30. GB 175-2007; Common Portland Cement. Standard Press of China: Beijing, China, 2007.
31. GB/T 19923-2005; The reuse of urban recycling water—water quality standard for industrial uses. Standard Press of China: Beijing, China, 2005.
32. GB 50119-2013; Code for concrete admixture application. Standard Press of China: Beijing, China, 2013.
33. GB/T50080-2016 Standard for Test Method of Performance on Ordinary Fresh Concrete, Standard Press of China: Beijing, China, 2016.
34. HJ/T 299-2007; Solid Waste-Extraction Procedure for Leaching Toxicity-Sulfuric Acid & Nitric acid Method. Standard Press of China: Beijing, China, 2007.
35. HJ 77.4-2008; Soil and sediment determination of polychlorinated dibenzo-p-dioxins (PCDDs) and polychlorinated dibenzofurans (PCDFs) by isotope dilution HRGC-HRMS. Standard Press of China: Beijing, China, 2008.
36. Jin, L.; Chen, M.; Wang, Y.; Peng, Y.; Yao, Q.; Ding, J.; Ma, B.; Lu, S. Utilization of mechanochemically pretreated municipal solid waste incineration fly ash for supplementary cementitious material. *J. Environ. Chem. Eng.* **2023**, *11*, 109112. [[CrossRef](#)]
37. Liu, J.; Xie, G.; Wang, Z.; Zeng, C.; Fan, X.; Li, Z.; Ren, J.; Xing, F.; Zhang, W. Manufacture of alkali-activated cementitious materials using municipal solid waste incineration (MSWI) ash: Immobilization of heavy metals in MSWI fly ash by MSWI bottom ash. *Constr. Build. Mater.* **2023**, *392*, 131848. [[CrossRef](#)]
38. Wen, J.R.; Liu, X.T.; Liu, K.P.; Gao, N.; Zhong, J.Q.; Sun, Z.H.; Wang, S.Y. Study on clay coal gangue strengthening technology. *Bull. Chin. Ceram. Soc.* **2020**, *39*, 233–241.
39. Zhao, Z.F.; Peng, B.Y.; Shao, G.H. Effects of cementation solution parameter on reinforcing silt by bio-cementation. *J. Southeast Univ. (Nat. Sci. Ed.)* **2021**, *51*, 456–462.
40. Zhou, W.Y.; Liu, J.K. Mechanical properties of compacted loess pretreated with calcium chloride. *Highway* **2021**, *66*, 291–295.
41. Trezza, M.A.; Lavat, A.E. Analysis of the system  $3\text{CaO}\cdot\text{Al}_2\text{O}_3\text{-CaSO}_4\cdot 2\text{H}_2\text{O}\text{-CaCO}_3\text{-H}_2\text{O}$  by FT-IR spectroscopy. *Cem. Concr. Res.* **2001**, *31*, 869–872. [[CrossRef](#)]
42. Richard, T.; Mercury, L.; Poulet, F.; d’Hendecourt, L. Diffuse reflectance infrared Fourier transform spectroscopy as a tool to characterise water in adsorption/confinement situations. *J. Colloid Interface Sci.* **2006**, *304*, 125–136. [[CrossRef](#)] [[PubMed](#)]

43. Liu, C.B.; Ji, H.G.; Liu, J.H.; He, W.; Gao, C. Experimental study on slag composite cementitious material for solidifying coastal saline soil. *J. Build. Mater.* **2015**, *18*, 82–87.
44. Wang, C.L.; Ni, W.; Li, D.Z.; Geng, B.Y.; Wu, H. Experimental study of using shanxi lingqiu low-silica iron ore tailings to produce aerated concrete. *J. China Coal Soc.* **2012**, *37*, 1129–1133.
45. Gou, M.F.; Guan, X.M.; Zhang, H.B. Chloride binding in monosulfaluminate hydrate. *J. Build. Mater.* **2012**, *15*, 863–866.
46. Lu, Q.M.; Zhang, Y.X.; Zhang, R.L.; Wu, J.G. Mechanical properties and microscopic analysis of coal bottom ash-fly ash cementitious system. *J. Henan Polytech. Univ. (Nat. Sci.)* **2019**, *38*, 140–145.
47. GB 5085.7-2019; Identification standards for hazardous waste: General rules. Standard Press of China: Beijing, China, 2019.
48. HJ 1134-2020; Technical specification for pollution control of fly-ash from municipal solid waste incineration. Standard Press of China: Beijing, China, 2020.
49. GB 30760-2014; Technical specification for coprocessing of solid waste in cement kiln. Standard Press of China: Beijing, China, 2014.
50. Xue, J.C.; Huang, Q.F.; Yang, Y.F. Distribution of Cr, As and Pb in cement mortar determined by electron probe microanalysis. *Acta Sci. Circumstantiae* **2011**, *31*, 798–804.
51. Wang, Y.S.; Huang, D.J.; Chen, J.X.; Chen, X.Y.; Yang, W.C. Distribution of pcddfs in soil before and after operation of municipal solid waste incinerator. *Res. Environ. Sci.* **2020**, *33*, 1938–1945.
52. Chen, X.C.; Yao, C.C.; Zhao, T.; Xu, J.Y.; Bu, Y.; Zhang, W.Q.; Liu, Y.Y.; Diao, G.W.; Zhang, J.Y. Immobilization remediation of Cr-contaminated soils by hydrocalumite and the relevant risk assessment. *China Environ. Sci.* **2021**, *41*, 1790–1798.
53. GB 5085.3-2007; Limit Values of Hazardous Waste Identification Standards. Standard Press of China: Beijing, China, 2007.

**Disclaimer/Publisher’s Note:** The statements, opinions and data contained in all publications are solely those of the individual author(s) and contributor(s) and not of MDPI and/or the editor(s). MDPI and/or the editor(s) disclaim responsibility for any injury to people or property resulting from any ideas, methods, instructions or products referred to in the content.